High-Isolation Dual-Polarized Leaky Wave Antenna With Fixed Beam for Full-Duplex Millimeter-Wave Applications

Ye, Qi-Cheng; Zhang, Yiming; Li, Jia-Lin; Pedersen, Gert Frølund; Zhang, Shuai

Published in:
I E E E Transactions on Antennas and Propagation

DOI (link to publication from Publisher):
10.1109/TAP.2021.3109592

Publication date:
2021

Document Version
Accepted author manuscript, peer reviewed version

High-Isolated Dual-Polarized Leaky Wave Antenna With Fixed Beam for Full-Duplex Millimeter-Wave Applications

Qi-Cheng Ye, *Student Member, IEEE*, Yi-Ming Zhang, *Member, IEEE*, Jia-Lin Li, Gert Frølund Pedersen, *Senior Member, IEEE*, and Shuai Zhang, *Senior Member, IEEE*

***Abstract*—In this paper, a high-isolated dual-polarized leaky-wave antenna (LWA) with a fixed beam is proposed for full-duplex millimeter-wave applications. The proposed antenna consists of a dual-polarized LWA array and an orthogonally differential feeding network. The proposed dual-polarized LWA array is developed based on the proposed LWA unit cell, which is suitable for differential feed, and the open-stop band is eliminated. The proposed feeding network provides two pairs of orthogonally differential excitation for the LWA array to realize the fixed beam with orthogonal polarization in boresight direction; the high inter-port isolation is implemented as well. The prototype for demonstration purposes is fabricated and measured. The measured results show that the proposed antenna exhibits an operating band from 27.6 GHz to 29.5 GHz with a maximum gain of up to 24 dBi. Furthermore, the measured inter-port isolation is higher than 51 dB within the operating band, where the maximum isolation is up to 60 dB. The measured cross-polarization levels are also very low, less than −27 dB. The proposed antenna features high gain, high inter-port isolation, and good co/cross-polarization isolation, achieving a good Tx/Rx separation for the in-band full-duplex applications at millimeter-wave frequencies.**

***Index Terms*—High isolation, high gain, leaky-wave antenna, dual-polarization, full-duplex, millimeter-wave.**

I. Introduction

RECENTLY, the in-band full-duplex (IBFD) applications show considerable potential in improving spectral efficiency [1]. The IBFD applications can use the same frequencies to simultaneously transmit and receive (STAR) signals. Thus, the cancellation of the self-interference between the local transmitter (Tx) and receiver (Rx) is essential. In general, a total isolation level of over 110 dB between Tx and Rx is required for the IFBD system [2], which can be synthetically achieved in antenna, analog, and digital layers. As for the antenna layer, the isolation should be as high as possible [3], [4]. For instance, an isolation level higher than 50 dB can effectively decrease the burden of analog and digital layers (only a 30 dB isolation level is required for each analog and digital layer). Moreover, millimeter-wave (mm-wave) frequencies have large spectrum resources for high data rate communications. Due to the high path loss in mm-wave bands, antennas/arrays are required to have high gain to compensate for the loss [5]. Therefore, mm-wave antenna designs with high isolation in Tx/Rx and high gain attract considerable interest.

The separation of Tx and the local Rx antennas is a simple scheme to improve the inter-port isolation, the straightforward methods such as antenna diversity [6], [7], polarization diversity [7], decoupling structure [8], all at the cost of bulky systems. Therefore, the shared-aperture antenna system for Tx and Rx might be more attractive for miniaturization purposes. In general, two main aspects are used for the shared-aperture scheme, i.e., beamforming network (BFN) and orthogonal-polarization based approaches. The former aims at the design of a multiport network to excite the antenna system for achieving a high isolation performance [9]-[15]. For example, in [9]-[12], many co-circularly polarized antennas are presented. By using BFNs to feed the antenna system with an orderly phase and magnitude distribution, the Tx/Rx antenna can operate in the same polarization, and high isolation is implemented. Besides, several omnidirectional antennas for STAR with vertically or horizontally polarized radiation are proposed [13]-[15], the BFNs are also used. Note that the employed multiport BNFs in these designs are mainly studied and realized at low frequencies (e.g., Sub-6 GHz bands). To keep a high self-interference suppression level, extremely small magnitude and phase imbalances between the output ports are generally essential [9], leading to complicated design procedures and bulky systems. This might not be effective for mm-wave applications, since physical sizes are limited and the small phase imbalance is very challenging to control for multiport networks at high frequencies.

For the orthogonal-polarization based approaches, the different polarizations are respectively used for Tx and Rx antennas, since the natural isolation exists between the orthogonal linear polarization [16]. Furthermore, the differential feed technique can be adopted to further enhance

This work was supported by AAU Young Talent Program. (Corresponding author: *Shuai Zhang*)

Q. -C. Ye is with the School of Physics, University of Electronic Science and Technology of China, Chengdu 611731, China, and also with the Antenna, Propagation and Millimeter-wave Systems (APMS) Section, Aalborg University, 9220 Aalborg, Denmark (e-mail: qichengye@std.uestc.edu.cn).

Y.-M. Zhang, G. F. Pedersen and S. Zhang are with the Antenna, Propagation and Millimeter-wave Systems (APMS) Section, Aalborg University, 9220 Aalborg, Denmark (e-mail: yiming@es.aau.dk; gfp@es.aau.dk; sz@es.aau.dk).

J. -L. Li is with the School of Physics, University of Electronic Science and Technology of China, Chengdu 611731, China (e-mail: jialinli@uestc.edu.cn).

isolation [17]-[24]. In [17], by using two 3-dB 180°-couplers to feed a patch antenna orthogonally, a Tx/Rx isolation of 90 dB in 20 MHz bandwidth at around 2.4 GHz was obtained. Nevertheless, the required external couplers leading to a bulky volume, and some relevant designs show in [19]-[21] are also incompact. In [19], a traveling-wave patch array operating at 15 GHz was fed by orthogonally differential excitations from two external baluns. However, the scheme is not suitable for mm-wave systems due to the high insertion loss and parasitic effect resulting from dozens of matched resistors on the array center. The dual-polarized antennas mentioned above mainly focus on low-frequency systems. Several dual-polarized mm-wave antennas with high isolation were reported [25], [26]. Benefiting from the natural isolation of orthogonal polarization, the isolation in [25] is higher than 35 dB. As for the one given in [26], the achieved isolation is up to 50 dB. However, the design with multi-layered feeding network in [26] is quite complicated. A small number of dual-polarized mm-wave antenna based on differential feed are also reported. For instance, in [27], the antenna is driven by two pairs of microstrip differential feed, the realized isolation is great than 35 dB within the entire operating bands. In general, most of the recently reported mm-wave antennas have the inter-port isolation below 50 dB [28]-[30], the dual-polarized mm-wave antenna design with high isolation and high gain is still a key challenge.

On the other hand, the leaky-wave antenna (LWA) gains significant interest in beam scanning applications due to the inherent capability of beam scanning without any additional feeding network [31], [32]. Recently, to realize a narrow beam on both E-plane and H-plane, several transversal long slot (or metal strip) LWA designs with finite periods were reported [33]-[37]. In [34]-[36], a scheme for fixed beam applications is proposed. Different from the conventional LWA, a pair of differential signals is used to excite two sides of the LWA to realize the fixed beam. However, the design suffers the open-stop band (OSB) in the boresight direction, which means the signals would be almost reflected, and radiation power would sharply reduce [31]. Therefore, the synthetic beam is only formed within a narrower bandwidth outside the stopbands.

To develop the potential of the mm-wave in full-duplex communication, a high isolated dual-polarized LWA with a fixed beam is presented in this paper. An improved LWA unit cell is proposed to eliminate the OSB under differential feed. More detailed, the operation mechanism of the presented one-dimensional (1-D) LWA array under differential feed is also analyzed, and a two-dimensional (2-D) planar dual-polarized LWA array is further developed. Based on the orthomode differential coupler (ODC) and the pillbox transitions, a quasi-TEM planar wave differential feeding network is presented and elegantly integrated with the dual-polarized LWA array. Finally, a prototype is fabricated and measured to verify the performance. Compared to the recently published works, the contributions and advantages of this design can be listed as follows:

a) An improved LWA unit cell with long transverse slots is proposed for differential feed where the OSB is addressed.

b) A 2-D dual-polarized LWA array with differential feed is further constructed, featuring high gain in boresight direction (without the OSB) and high polarization purity in radiation patterns.

c) The proposed orthogonal differential feeding network is quite simple with low insertion loss. Owing to the symmetry of the structure, very low magnitude and phase imbalances are achieved, resulting in a high self-interference suppression level.

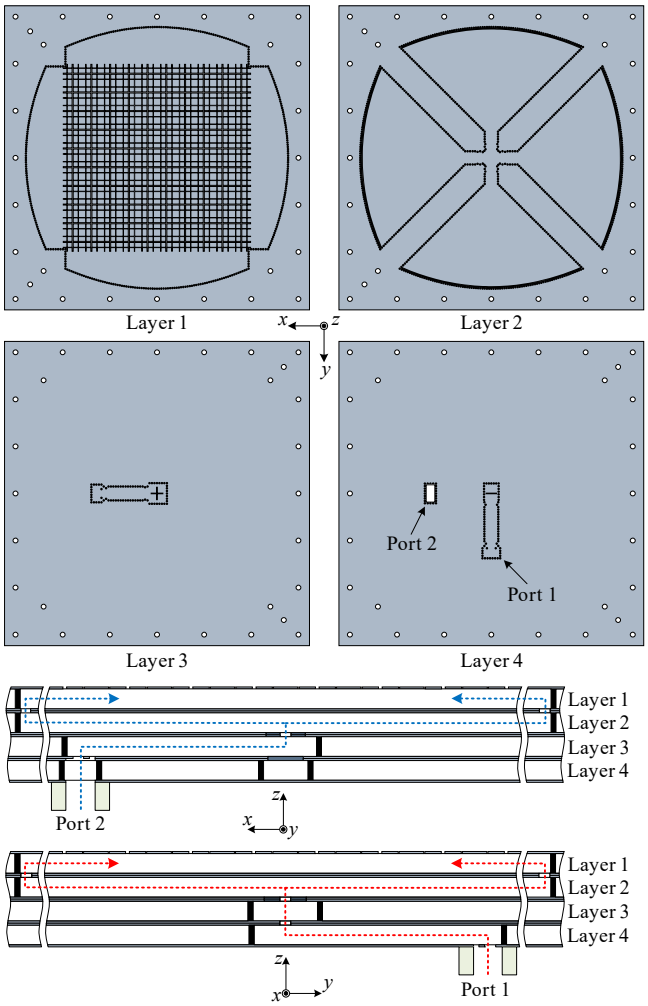

Fig. 1. Configuration of the proposed dual-polarized LWA antenna.

II. Antenna Design and Analysis

The configuration of the proposed dual-polarized antenna operating at 28 GHz is shown in Fig. 1, it consists of four layers Rogers RO3003 with a dielectric constant of 3.0, and the thickness of each layer is 0.762 mm. All layers are fixed together with screws located at the edge of the antenna aperture. The orthogonal LWA slot array is etched at the top surface of layer 1. For each polarization, there are ten periods of unit cells. Layer 2, 3, and 4 construct the feeding network for the dual-polarized LWA array. By integrating the ODC and four pillbox transition systems, two pairs of orthogonal differential quasi-TEM planar waves for the LWA array can be generated. Two standard WR-28 rectangular waveguides are used for the

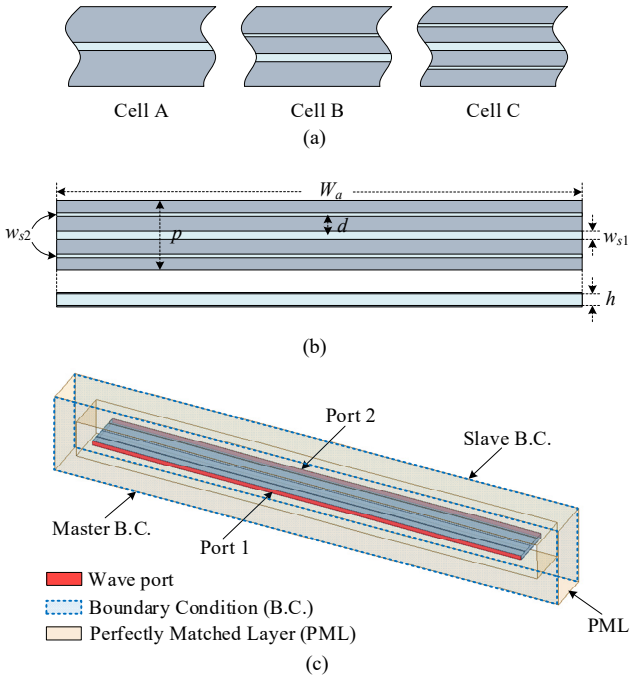

Fig. 2. (a) Different kinds of the unit cell. Cells A and B have the same dimensions as Cell C except for the period of Cell A is 6.9 mm. (b) Specific design of the proposed symmetrical unit cell (Cell C). (c) Simulation model of the single unit cell with periodic boundary condition. The wave ports excite the dominant mode, and PML surrounds the unit cell in the directions perpendicular to the excitation.

TABLE I
DIMENSIONS OF PROPOSED UNIT CELL (UNITS: mm)

Par.	W_a	p	d	w_{s1}	w_{s2}	h	L_a
Val.	76.8	7.68	2.28	0.45	0.13	0.762	76.8

excitation of two orthogonal polarized radiation, respectively.

When the ports are excited, the ODC composed in Layer 2, 3, and 4, transforms the input electromagnetic (EM) waves into two pairs of differential signals in *x*- and *y*-directions (see blue and red dashed lines). Then, these signals are transmitted to the dual-layers (Layer 1, 2) pillbox transition systems, where the TE_{10} mode wave is further converted to a quasi-TEM planar wave to excite the LWA array. The full-wave simulations were performed by the commercial software CST 2019.

A. Selection of LWA Unit Cell for Differential Feed

In this design, the differential feed means each unit cell of the LWA array will receive the excitation signals from both sides with 180° phase differences. Significantly, only the useable conventional feed can realize the differential feed. To achieve the broadside and symmetrical radiation patterns, the same excited responses of two differential ports for unit cells are required. Fig. 2(a) shows three kinds of LWA unit cells with long transversal slots. Cell A is the conventional design with a single slot, while Cell B has two asymmetrical slots with different widths [31], [37]. The proposed symmetrical Cell C with three slots is shown in Fig. 2(b), in which a wider slot is situated on the center, and two same narrower slots are symmetrically set on both sides. The optimized dimensions are given in Table I. The simulation model is illustrated in Fig. 2(c).

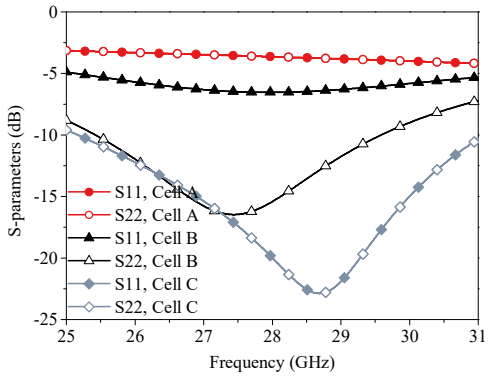

Fig. 3. S parameter response of the different unit cells based on full-wave simulation.

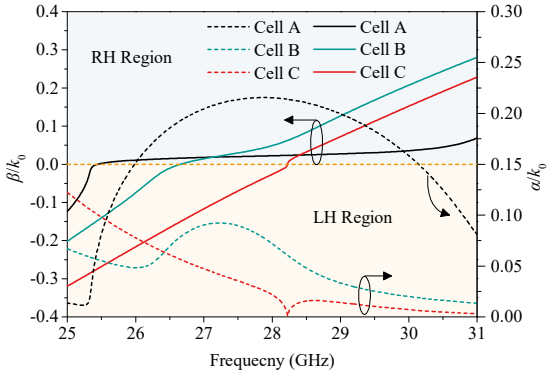

Fig. 4. Normalized phase and attenuation constants of the different unit cells based on full-wave simulation.

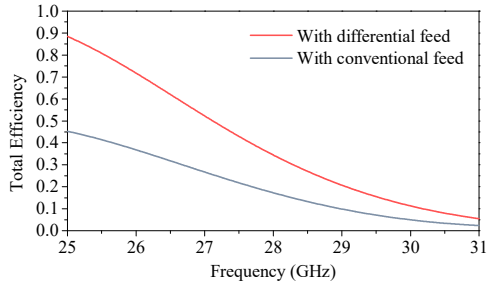

Fig. 5. Simulated total efficiency of the single proposed unit cell with conventional and differential feed.

Fig. 3 depicts the reflection coefficients of two ports for each unit cell. When one port is excited, the other one is terminated with a matched load, i.e., conventional feed mode. As seen, the identical responses can be obtained from both sides for the symmetrical structure, namely Cells A and C but not Cell B. This result indicates that Cell B cannot apply to the differential feed as the different response means asymmetrical radiation characteristic.

On the other hand, Fig. 4 illustrates the normalized phase constant β and attenuation constant α of three kinds of unit cells based on full-wave simulation. It is observed that a good balance between left-hand (LH) and right-hand (RH) region is found in Cell C, which means the OSB is almost eliminated. The OSB is also mitigated a lot in Cell B, which benefits from the asymmetrical double slots. However, the normalized phase constant β of Cell A is much closer to zero within wide bands due to the suffered OSB [31]. The phase constant does not

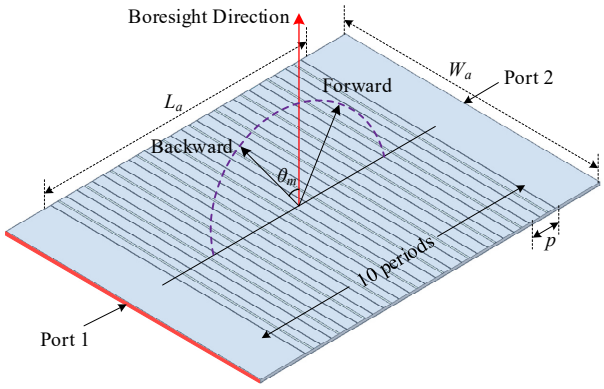

Fig. 6. 1-D periodic LWA array.

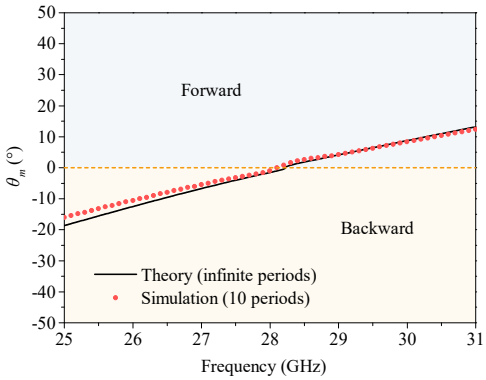

Fig. 7. Beam directions of the 1-D periodic LWA array with conventional feed.

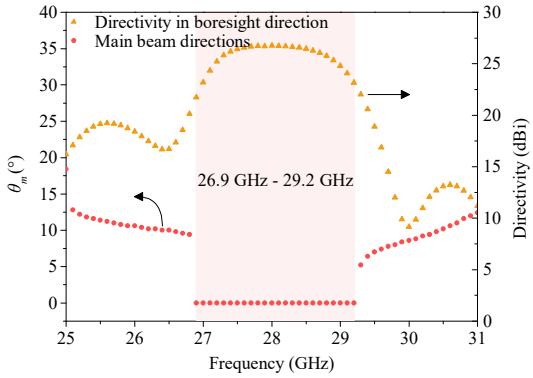

Fig. 8. Main beam directions versus frequencies and directivity in boresight direction with differential feed.

exactly equal zero as this structure contains the open slot.

Moreover, the normalized attenuation constant of Cell C has a relatively smooth and stable curve instead of Cells A and B. This is significant for differential feed since the suitable attenuation constant can lead to a favorable amplitude distribution in LWA array, the detailed analysis is presented in Section II-B. The phase constants and attenuation constants are extracted by using the following expressions [38]:

$$\beta = \frac{1}{p} \cdot \mathrm{Im}\left(\cosh^{-1}\left(\frac{1 - S_{11}S_{22} + S_{12}S_{21}}{2S_{21}} \right) \right) \tag{1}$$

$$\alpha = \frac{1}{p} \cdot \mathrm{Re}\left(\cosh^{-1}\left(\frac{1 - S_{11}S_{22} + S_{12}S_{21}}{2S_{21}} \right) \right) \tag{2}$$

where the S parameters are obtained by simulating a single unit cell as a two-port network. Note that the full-wave simulation results for unit cells in this paper, the periodic boundary condition (B. C.) was applied to accurately contain the coupling effect between the adjacent unit cells.

Comparing with Cells A and B, it can be concluded that only the proposed Cell C can be used for the differential feed due to the efficient mitigation of the OSB and the symmetrical radiation response. The same conclusion can also be obtained from Bloch impedance analysis.

The total radiation efficiency of the proposed Cell C is studied. Fig. 5 shows the full-wave simulation results with conventional and differential feed. It is observed that the radiation efficiency with differential feed is higher than the conventional within the whole band. This result indicates that the standing-wave formed by differential feed efficiently facilitates the slot radiation.

B. *Analysis of LWA Array*

Based on the proposed unit cell, a one-dimensional (1-D) periodic linearly polarized LWA array with 10 periods is proposed, as shown in Fig. 6. The conventional feed for the proposed LWA array is firstly considered. Namely, port 1 is excited with the quasi-TEM planar wave, while port 2 is connected to a matched load. According to the study of LWA theory [39], the angle of maximum directivity $\theta_m(f)$ (main beam direction) and the 3-dB beamwidth $\Delta\theta(f)$ versus frequency can be approximated by (3) and (4), respectively.

$$\theta_m(f) \approx \sin^{-1}\left(\frac{\beta(f)}{k_0} \right) \tag{3}$$

$$\Delta\theta(f) \approx \frac{1}{(L_a / \lambda_0)\cos\left[\theta_m(f)\right]} \tag{4}$$

where the k_0 is the free-space wavenumber, L_a is the length of the LWA antenna, and λ_0 is the free-space wavelength. According to (3), the theoretical angle of the main beam direction is curved in Fig. 7 based on the normalized phase constant $\beta(f)/k_0$. The main beam scan from backward to forward direction is observed, in which the frequency at boresight direction (0°) is called balanced point f_b. Moreover, the main beam directions versus frequencies obtained by full-wave simulation are also depicted, and it is generally consistent with the theoretical result.

To realize the broadside radiation, port 1 and port 2 are excited with a pair of differential signals. Subsequently, two co-polarized scanning beams are generated, which are respectively pointed to the forward and backward direction. It can be expected that when two symmetrical beams are approaching the boresight direction, they superposition together to form a single beam and pointed to the boresight direction. This capability works in the bands of f_l to f_h ($f_l < f_b < f_h$), as the two beams are always scanning near the boresight direction. As shown in Fig. 8, the main beam directions and the directivity in the boresight direction versus the frequency are depicted (the frequency step is 0.1 GHz). As seen, the main beam is maintained in boresight direction with directivity values of higher than 21.7 dBi from 26.9 GHz to 29.2 GHz. When the frequency departs away from the operation band, the

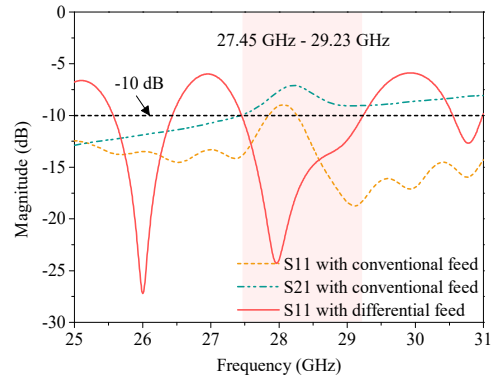

(a)

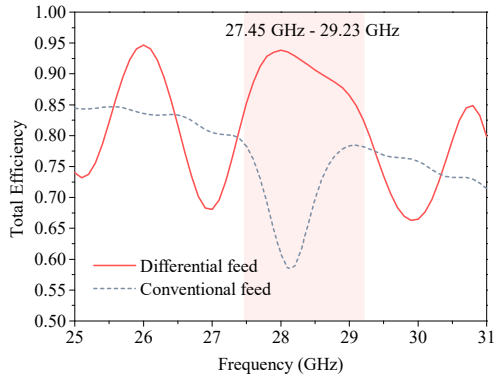

(b)

Fig. 9. Simulated performance of 1-D LWA array excited by the conventional and the differential feed. (a) S-parameters. (b) Total efficiencies.

directivity is sharply decreased, and the main beam no longer appears in the boresight direction. These results indicate that the synthetic beam is only formed within a limited scan range, corresponding to the [−6.0°, 5.0°] in Fig. 7. The variation of phase constant as the frequency is the dominant factor to affect the synthetic beam. A more stable variation can keep the scanning beam close to the boresight direction in a wider frequency band; thereby, a wider bandwidth of usable synthetic beam is obtained. The beamwidth is the other factor that affects the synthetic beam. From (4), a longer length of the LWA leads to a narrower main beam. At this point, the symmetrical beams should further be close to the boresight direction to gain the usable synthetic beam, which results in the usable bandwidth would be further reduced.

Fig. 9(a) shows the S parameters of the 1-D LWA, which are excited by the conventional and differential feeds. Seeing that the used unit cell does not achieve the optimum balance condition, the reflection coefficient is higher than −10 dB with the conventional feed. After employing the differential feed, the result shows the LWA array is matched well within the band of 27.45 - 29.23 GHz. Besides, as shown in Fig. 9(b), the total efficiency with differential feed is higher than 83% in the whole impedance bandwidth (27.45 GHz - 29.23 GHz), the maximum is up to 94%. As for the conventional feed, it is lower than 60% from 28.1 GHz to 28.2 GHz. It can be concluded that the total efficiency with differential feed in the impedance bandwidth is higher than that with conventional feed if the number of the periods is the same.

When two antiphase traveling-waves propagate in opposite directions in the LWA, the standing-waves are formed when they meet. Since the EM wave is continuously radiated when moving forward, the amplitude from the excitation end to the other end will gradually decrease. This leads to the strongest standing-wave amplitude in the central area of the LWA and weaker amplitude to the sides. In contrast, the strongest traveling-waves are located on the two excitation sides. The voltage at the mid-point of the LWA will always be zero, and this point is one of the wave nodes of the standing-waves. Due to the formed standing-waves greatly facilitating the radiation of the open slots (see Fig. 5), so that the total radiation efficiency of the LWA array is greatly enhanced, and a lower reflection is also realized.

Moreover, to increase the total efficiency of the LWA array, the favorable distribution of the standing-waves and traveling-waves is very significant. This distribution can be controlled by the attenuation constant (or radiation efficiency) of the single unit cell and the number of the periods. Therefore, the number of periods in this design is preferably set as 10 to obtain high total efficiency and low reflection coefficient. Note that the unit cell may not achieve perfect balance conditions due to parameter optimization, but it is acceptable for the differential feed, as shown in Fig. 9(a). Although the standing-waves appear inside the LWA array, the classical design rules of the LWA are not changed, which is because a standing-wave can be decomposed to a pair of antiphase traveling-waves.

By integrating two identical 1-D periodic LWA arrays with the orthogonal arrangement, the planar dual-polarized LWA array with grid slots is proposed, as shown in Fig. 1. Each polarization is with a pair of differential ports. In this way, the dual-polarized broadside radiation can be realized. The feeding network is presented in Section III.

III. Design of Feeding Network

In this design, the feeding network for the radiation Layer 1 (see Fig. 1) is integrated into Layers 2, 3, and 4, by employing an ODC and four pillbox transition systems. Two pairs of differential feed with quasi-TEM planar wave for Layer 1 are realized.

A. Orthomode Differential coupler (ODC)

Fig. 10 illustrate the configuration of ODC with a three-layer stack, and the dimensions are listed in Table II. An ODC based on a two-layered structure is also reported in [40]. However, the isolation between the input ports is around 18 dB. In contrast, the presented ODC in this work is a crucial component, which provides a high inter-port isolation for the proposed dual-polarized LWA array. As shown in Fig. 10, Layer 2 is the orthomode transducer (OMT) with a crossed coupling slot etched on the bottom. Layer 3 and Layer 4 are the feeding layers, which correspond to each orthomode, respectively. When the ODC is excited by port 2, the signals are coupled to the OMT through the transverse coupling slot, and then the signals are equally divided to port 2a and 2b with a 180° phase difference. Here, as the transverse channel is exactly

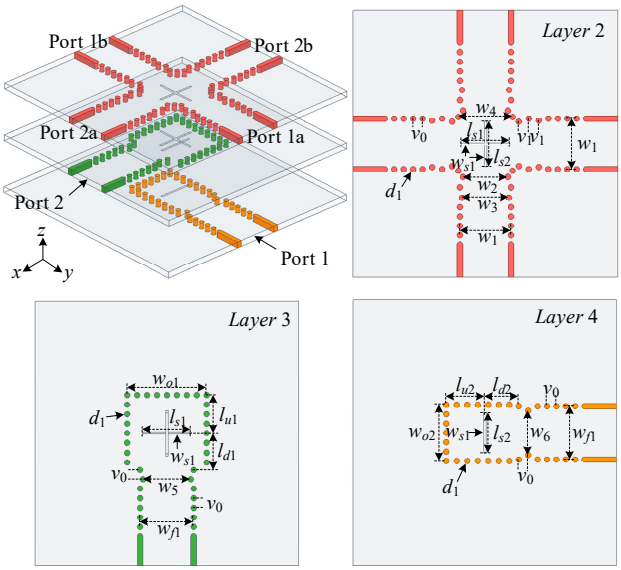

Fig. 10. Configuration of the ODC.

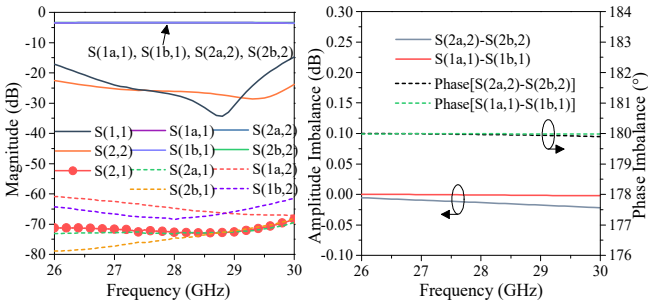

Fig. 11. Simulated performance of the ODC. (a) S parameters. (b) Amplitude imbalance and phase imbalance.

TABLE II
DIMENSIONS OF PROPOSED ODC (UNITS: mm)

Par.	w_1	w_2	w_3	w_4	w_5	w_6	v_0
Val.	5.4	4.74	4.96	5.73	5.08	4.72	1
Par.	v_1	l_{s1}	l_{s2}	l_{s3}	w_{s1}	d_1	w_{o1}
Val.	1.06	5.12	4.8	4.28	0.25	0.6	8.45
Par.	w_{o2}	w_{f1}	l_{d1}	l_{d2}	l_{u1}	l_{u2}	
Val.	6	5.7	3.86	3.61	4.08	4.1	

orthogonal with the longitudinal one, only a tiny amount of power of EM waves is parasitically leaked into the differential ports 1a and 1b. Different from port 2, the signals excited by port 1 are first coupled to Layer 3 and then Layer 2. Similarly, the signals from port 1 are equally divided to ports 1a and 1b with antiphase, while only tiny leakage signals exist in the longitudinal channel of the OMT. Since the signals excited by port 1 and port 2 are completely orthogonal, high isolation is implemented between the input ports, and two pairs of independent differential signals are generated in the transverse and longitudinal channels, respectively.

Fig. 11(a) shows the simulated S parameters of the ODC, it is seen the bandwidth of reflection coefficient below −20 dB is from 26.4 GHz to 29.5 GHz, where the coupling between the input ports is less than −71 dB. The signals leak to the isolated

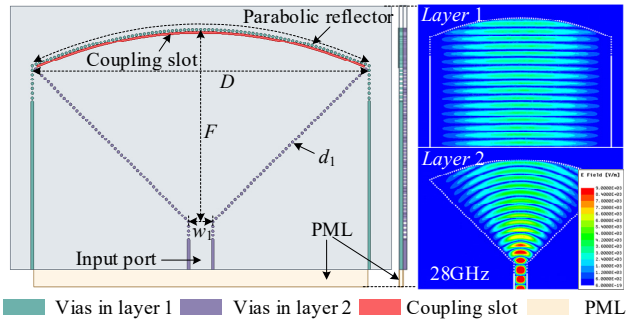

Fig. 12. Configuration of the pillbox transition system.

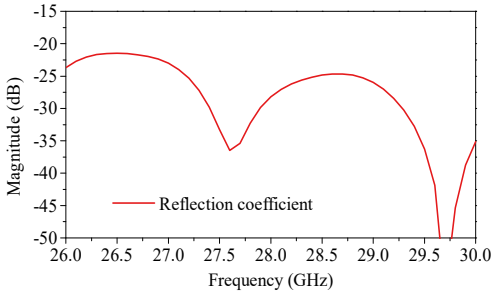

Fig. 13. Simulated reflection coefficient of the pillbox transition system.

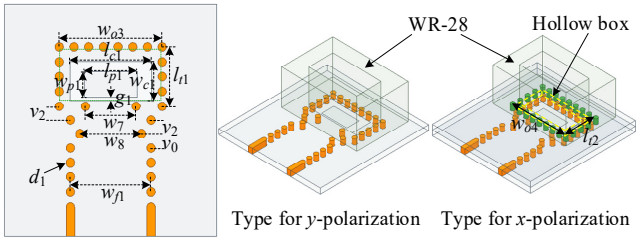

Fig. 14. Configurations of the employed two input transitions.

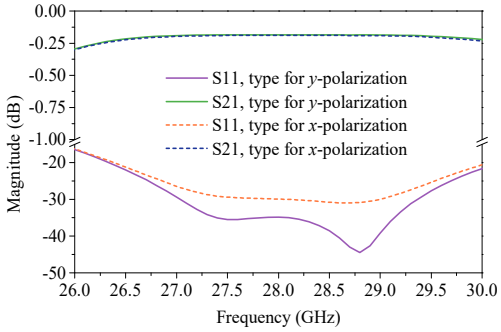

Fig. 15. Simulated performance of the waveguide to SIW transition.

TABLE III
DIMENSIONS OF PILLBOX TRANSITION AND INPUT TRANSITIONS (UNITS: mm)

Par.	D	F	w_7	w_8	v_2	l_{c1}	w_{c1}
Val.	75.1	43	3.58	4.36	0.95	5.78	2.69
Par.	l_{p1}	w_{p1}	w_{o3}	l_{t1}	w_{o4}	l_{t2}	g_1
Val.	3.73	1.8	7.28	4.12	8.11	4.56	0.21

output ports are lower than −60 dB for both two input ports. The amplitude and phase imbalance of output differential signals are given in Fig. 11(b), the amplitude imbalance is less than ±0.025 dB in both transverse and longitudinal channels, and the phase imbalance is also less than ±0.03°.

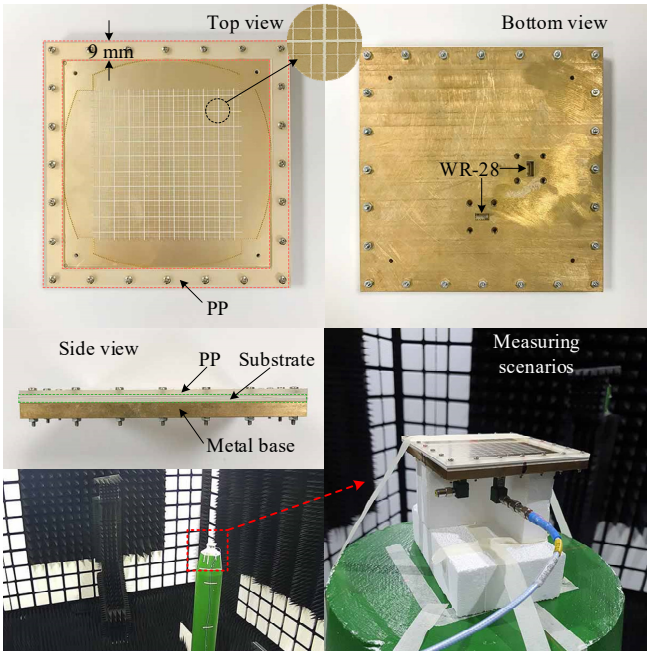

Fig. 16. Fabricated prototype and the measuring scenario.

B. Pillbox Transition System

When the signals enter four pillbox transition systems from ODC, the TE_{10} wave is converted into the quasi-TEM planar wave to feed the LWA array. Fig. 12 shows the configuration of the single pillbox transition system, which is constructed in Layer 1 and Layer 2, and the parameters are listed in Table III. In this structure, the parabolic reflector is built by the metallic vias array with small spacing. It is connected with the open-ended SIW by a similar metallic vias array. The closed boundary can reduce the leakage of the EM wave. Parabolic slots are etched on both the bottom of Layer 1 and the top of Layer 2 to coupling the signals, and they have a width of 0.42 mm. The slots are only 0.1 mm away from the parabolic reflector. According to the width of the LWA array, the aperture D of the parabolic reflector is set as 75.1 mm. Due to the ratio of F/D that could affect the magnitude distribution of the generated quasi-TEM planar wave, the sidelobe level in the H-plane of the LWA would be further affected. Therefore, the F is preferably set as 43 mm in the final design to realize a low sidelobe level and a compact size. As seen in Fig. 13, the simulated reflection coefficient of the exciting port is below −21 dB within the whole frequency band. To obtain the optimal parameters, the PML is placed on the output port to absorb the generated quasi-TEM planar waves and the possible noise waves during the optimization simulation.

C. Input Transition

In this design, the WR-28 rectangular waveguides are used, and the transitions of the standard rectangular waveguide to the SIW are consequently indispensable. Fig. 14 shows two employed transitions, which are used for two orthogonal polarizations, respectively. Notably, different from the type for *y*-polarization provided in [41], a 0.762 mm-thick air-filled waveguide is added between the SIW end and feeding waveguide in type for *x*-polarization. The rectangular metallic vias array constructs the inserted waveguide, and the substrate inside the waveguide is removed to match the standard rectangular waveguide. The detailed dimensions are given in Table III. Fig. 15 shows that the achieved reflection coefficients of two transitions are lower than −21 dB in the band from 26.5 GHz to 30 GHz with the insert loss of less than 0.23 dB.

IV. Experiments and Comparison

To verify the proposed dual-polarized LWA array, a prototype is simulated, fabricated, and measured. Fig. 16 presents the assembled prototype. A brass base and a square plastic ring are used as fixtures, with a thickness of 7 mm and 2 mm, respectively. The WR-28 standard waveguide flange is fabricated in the metal base. Two metal dowels on the base are used to align each layer substrate. Besides, 24 vertical screws are used to fix all layers together as well as the metal base. In this way, the air gap can be eliminated efficiently. The substrates are fabricated by the standard single-layer PCB processing technique. The CNC technique fabricates the fixtures of the metal base and the plastic ring. The dielectric constant and the loss tangent of the plastic material is 2.27 and 0.0003 at 28 GHz, respectively. It is found that the plastic ring does not affect the antenna performance via a controlled experiment. Two coaxial-to-waveguide adaptors (FLANN 22094-KF20) are mounted on the bottom of the base so that the antenna can be connected to the measuring device.

A. Experiment Results

In the measurements, the S parameters were measured by the Keysight PNA network analyzer N5227B, the radiation patterns and gains were measured in the anechoic chamber as presented in Fig. 16. Fig. 17(a) shows the simulated and measured reflection coefficients. For the reflection coefficient below −10 dB, the simulated overlapped bandwidth ranges from 27.4 GHz to 29.4 GHz for port 1 and port 2, while the measured overlapped bandwidth is from 27.6 GHz to 29.5 GHz. It is observed that the reflection coefficients for both ports are slightly worse than −10 dB around 27.5 GHz and 29 GHz. The isolation between the input ports is shown in Fig. 17(b), where the measured isolation is larger than 51 dB in bands of 27.6 GHz to 29.5 GHz. The maximum isolation is up to 60 dB at 28.6 GHz. For the simulated result, the isolation is higher than 76 dB within the studied band. The visible discrepancy between the measured and simulated results is mainly due to the fabrication and manually assembling imperfection. Despite that, high isolation is still realized in this design.

The gain performances of the proposed antenna in the boresight direction are given in Fig. 17(c), the simulated gains of two ports are almost the same, and the maximum gain is around 25.5 dBi at 28 GHz. For the measured gains, they are more than 20.5 dBi for port 1 and more than 21.1 dBi for port 2, within bands of 27.6 GHz to 29.5 GHz. The maximum gain is 23.7 dBi at 28.6 GHz for port 1 and 24 dBi at 28.3 GHz for port 2. Note that the insertion loss (0.2 dB) from coaxial-to-waveguide adaptors has been calibrated. It can be seen that the measured gains are slightly lower than the

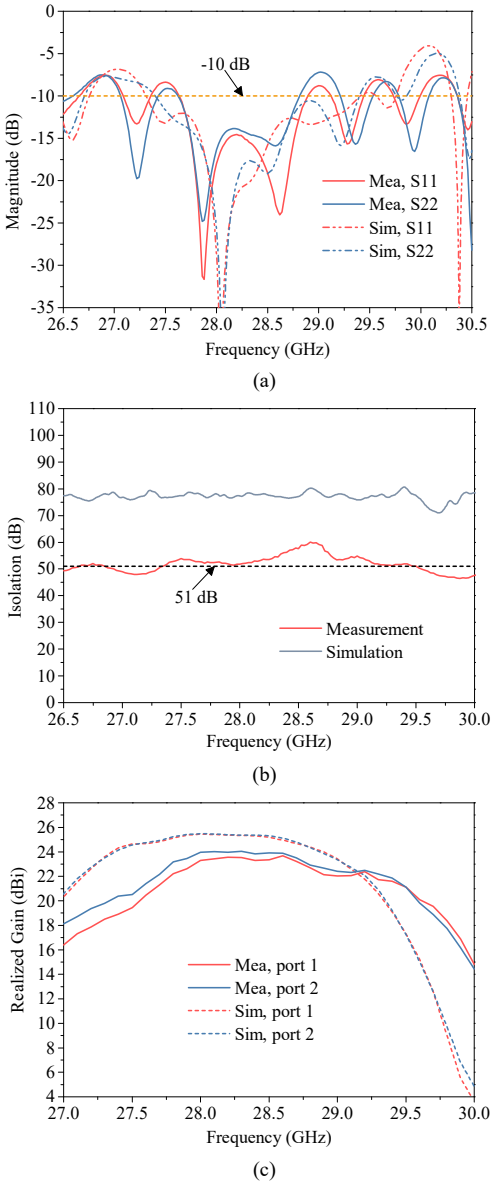

Fig. 17. Simulated and measured performances of the proposed antenna. (a) Reflection coefficients. (b) Isolation between input ports. (c) Gain performances.

simulated ones, and they are offset to the higher frequency by about 0.4 GHz compared to the simulations. During the manufacturing, the parameter variation of the LWA unit cell may lead to the shift of the phase constant resulting in the shift of gains.

Fig. 18 illustrates the far-field radiation patterns at 28 GHz, 28.5 GHz, and 29 GHz with port 1 excited. Due to the limitation of the facility, only the radiation patterns within −90° to 90° were measured. The measured patterns are in good agreement with the simulated, where the co-polarized radiation patterns are very symmetrical and directive. Besides, the simulated sidelobe level in the E-plane is below −13 dB, while the measured is lower than −11 dB. As for the H-plane radiation patterns, the sidelobe level is less than −18 dB in both simulations and measurements, which is contributed by the tapered amplitude distribution from the pillbox transition systems. As for the cross-polarization level, the simulated results are less than −60 dB, which is not visible in the figures. The measured results are below −27 dB in both two main planes, which is higher than simulated results due to the imperfection of the fabrication and manually assembling, as well as the limited test accuracy. Almost the same radiation patterns under the excitation of port 2 are presented in Fig. 19, which is no detailed for brevity.

B. *Comparison*

Recently published shared-aperture designs are summarized and listed in Table IV for comparisons. In terms of the critical performance of the isolation, it is found that the measured isolation of the proposed antenna is higher than all the listed designs. References [9] and [13] presented the designs with BFN that can also achieve good isolation. The key to these antennas is the practical performance of the BFN, particularly when extending to the array for a high gain, a more complicated BFN is inevitable. However, for mm-wave designs, the excellent amplitude and phase balance might be a challenge. As for the design in [19], the use of many matching resistors is impractical for mm-wave antennas due to the high-loss and parasitic effect. Moreover, the design in [9], [13], and [19] are usually required an additional space for the feeding baluns or BFNs, which would cause an incompact size or complicated overall structure. The designs in [24] and [25] have a comparatively simple structure without any additional devices, whereas the isolation performances are insufficient. Although measured isolation of up to 50 dB is presented in [26], the employed feeding network with a multi-layered metal structure is quite complicated, suffering decreased reliability, high cost, and heavyweight. In contrast, the proposed design has a simpler feeding structure than [26] and other designs. The proposed antenna also exhibits a good co/cross-polarization isolation, which is comparable to the other two mm-wave designs [25], [26]. In a word, the proposed antenna features high gain, high inter-port isolation, low cross-polarization level, and a simple feeding structure.

V. Conclusion

This paper presents a dual-polarized LWA with a fixed beam. The realized two orthogonal polarizations with high isolation can be used for full-duplex applications. In this design, the proposed symmetrical LWA unit cell is employed to develop the dual-polarized planar LWA array. The integrated feeding network provides an orthogonal differential quasi-TEM planar wave feed for the LWA array. The proposed antenna was fabricated and measured. The results show that the operating bandwidth is from 27.6 GHz to 29.5 GHz, and the measured maximum realized gain is up to 24 dBi. Moreover, symmetrical and unidirectional broadside radiation patterns are observed. In the operating band, the measured isolation of more than 51 dB between the two input ports is realized, and the maximum isolation is up to 60 dB. The elegant combination of LWA array and dual differential feed achieves high gain and high isolation, could be a valuable candidate for the mm-wave full-duplex applications.

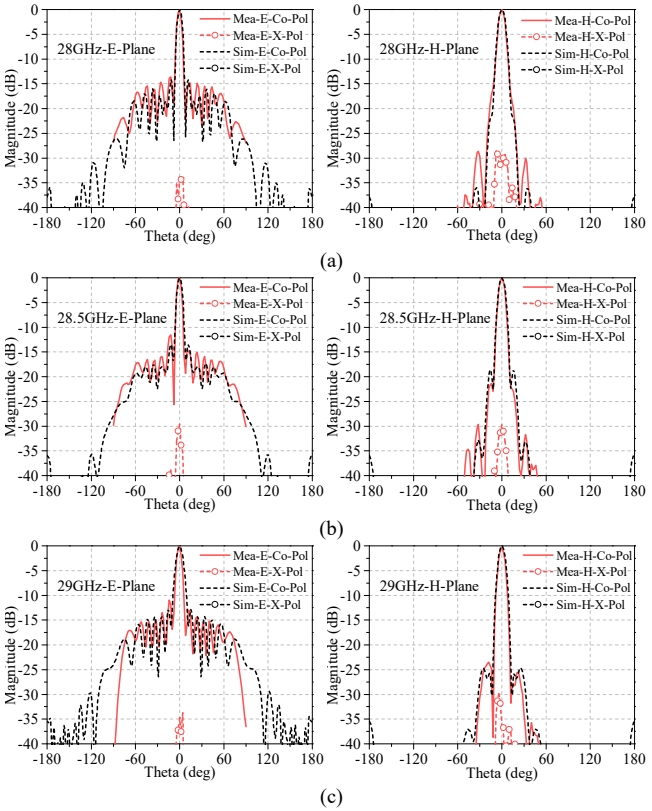

Fig. 18. Radiation patterns of the proposed antenna with port 1 excitation. (a) 28 GHz. (b) 28.5 GHz. (c) 29 GHz.

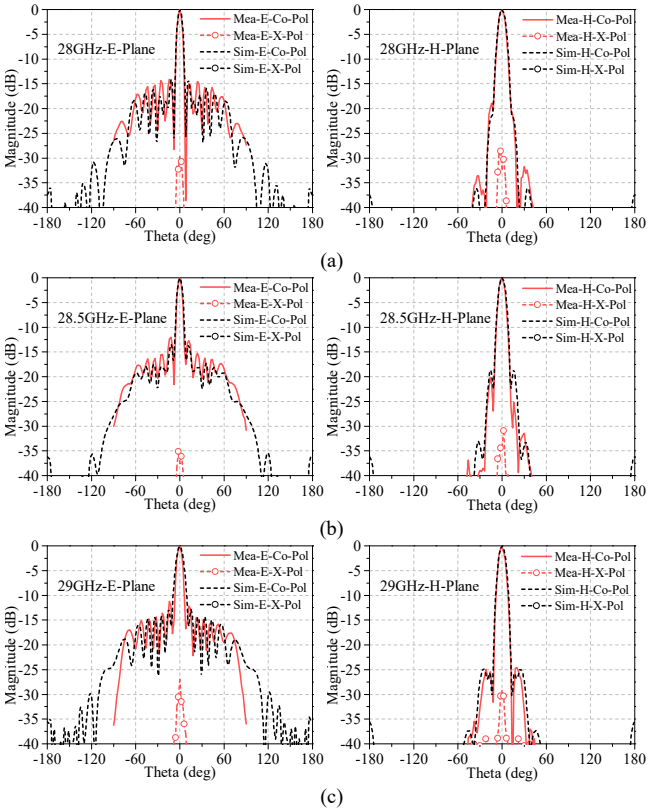

Fig. 19. Radiation patterns of the proposed antenna with port 2 excitation. (a) 28 GHz. (b) 28.5 GHz. (c) 29 GHz.

TABLE IV
COMPARISON BETWEEN PROPOSED ANTENNA AND REPORTED HIGH-ISOLATED DESIGNS

Ref.	Freq. (GHz)	Radi. Element	Decoupling Technique	Max Gain (dBi/dBic)	Antenna Size	Polarizations	Feeding Network Implementation	Co/X-Pol. Isolation. Mea.(dB)	Inter-port Isolation. Mea.(dB)
[9]	1.25-2.5	Archimedean spiral antenna	BFN	8.8 for Tx, 8.2 for Rx	Diameter:1.375λ_0 @ 1.875 GHz, height: 0.344λ_0	Co-CP	Complicated	9* for Tx 10* for Rx	>38
[13]	0.6-1.75	Monocone and bent loops	BFN	5.5 for Tx, 3.6 for Rx	Diameter:1.57λ_0 @ 1.175 GHz, height: 0.49λ_0	Co-VP	Complicated	10* for Tx 0* for Rx	>40
[19]	13.6-16	Patch	Orthogonal polarization + Differential feed	22.4	6.5λ_0×6.5λ_0×0.025λ_0 @ 15 GHz	Dual-pol	Complicated	40	>41*
[24]	11.98-15.42	Patch	Orthogonal polarization + Differential feed	N.A.	N.A.	Dual-pol	Simple	34	>32
[25]	55.7-66.1	Cavity-backed slot	Orthogonal polarization	22.3	10.4λ_0×10.4λ_0×0.5λ_0 @ 60 GHz	Dual-pol	Simple	19	>34.7
[26]	60-64	Cross sharped slot	Orthogonal polarization	32	14.8λ_0×14.8λ_0×1.5λ_0 @ 60 GHz	Dual-pol	Very complicated	26*	>50
This work	27.6 - 29.5	LWA slot	Orthogonal polarization + Differential feed	24	11.7λ_0×11.7λ_0×0.3λ_0 @ 28 GHz	Dual-pol	Very simple	27	>51

N.A.: Not available *: The values are obtained from the figures.

ACKNOWLEDGMENT

The authors would like to thank the lab engineer Kim Olesen for the support of the antenna measurements.

REFERENCES

[1] A. Sabharwal, P. Schniter, D. Guo, D. W. Bliss, S. Rangarajan, and R. Wichman, "In-band full-duplex wireless: challenges and opportunities," *IEEE J. Sel. Areas Commun.*, vol. 32, no. 9, pp. 1637-1652, Sept. 2014.
[2] D. Bharadia, E. McMilin, and S. Katti, "Full duplex radios," in *Proc. Int. Conf. ACMSIGCOMM*, Hong Kong, 2013, pp. 375–386.
[3] D. Korpi, M. Heino, C. Icheln, K. Haneda, and M. Valkama, "Compact

inband full-duplex relays with beyond 100 dB self-interference suppression: Enabling techniques and field measurements," *IEEETrans. Antennas Propag.*, vol. 65, no. 2, pp. 960–965, Feb. 2017.

[4] E. A. Etellisi, M. A. Elmansouri, and D. S. Filipovic, "Wideband monostatic simultaneous transmit and receive (STAR) antenna," *IEEE Trans. Antennas Propag.*, vol. 64, no. 1, pp. 6-15, Jan. 2016.

[5] D. Lockie and D. Peck, "High-data-rate millimeter-wave radios," *IEEE Microw. Mag.*, vol. 10, no. 5, pp. 75–83, Aug. 2009.

[6] Y. He, X. Yin, and H. Chen, "Spatiotemporal characterization of self-interference channels for 60-GHz full-duplex communication," *IEEE Antennas Wireless Propag. Lett.*, vol. 16, pp. 2220-2223, 2017.

[7] P. V. Prasannakumar, M. A. Elmansouri, and D. S. Filipovic, "Wideband decoupling techniques for dual-polarized bi-static simultaneous transmit and receive antenna subsystem," *IEEE Trans. Antennas Propag.*, vol. 65, no. 10, pp. 4991-5001, Oct. 2017.

[8] K. Iwamoto, M. Heino, K. Haneda, and H. Morikawa, "Design of an antenna decoupling structure for an inband full-duplex collinear dipole array," *IEEE Trans. Antennas Propag.*, vol. 66, no. 7, pp. 3763-3768, Jul. 2018.

[9] E. A. Etellisi, M. A. Elmansouri, and D. S. Filipovic, "Wideband monostatic co-polarized co-channel simultaneous transmit and receive broadside circular array antenna," *IEEE Trans. Antennas Propag.*, vol. 67, no. 2, pp. 843-852, Feb. 2019.

[10] E. A. Etellisi, M. A. Elmansouri and D. S. Filipović, "In-band full-duplex multimode lens-loaded eight-arm spiral antenna," *IEEE Trans. Antennas Propag.*, vol. 66, no. 4, pp. 2084-2089, Apr. 2018.

[11] Z. Zhou, Y. Li, J. Hu, Y. He, Z. Zhang, and P. Chen, "Monostatic copolarized simultaneous transmit and receive (STAR) antenna by integrated single-layer design," *IEEE Antennas Wireless Propag. Lett.*, vol. 18, no. 3, pp. 472-476, Mar. 2019.

[12] P. Valale Prasannakumar, M. A. Elmansouri, L. B. Boskovic, M. Ignatenko, and D. S. Filipovic, "Wideband quasi-monostatic simultaneous transmit and receive reflector antenna," *IEEE Trans. Antennas Propag.*, vol. 68, no. 4, pp. 2630-2637, Apr. 2020.

[13] R. Lian, T. Shih, Y. Yin, and N. Behdad, "A high-isolation, ultra-wideband simultaneous transmit and receive antenna with monopole-like radiation characteristics," *IEEE Trans. Antennas Propag.*, vol. 66, no. 2, pp. 1002-1007, Feb. 2018.

[14] L. Sun, Y. Li, Z. Zhang, and Z. Feng, "Compact co-horizontally polarized full-duplex antenna with omnidirectional patterns," *IEEE Antennas Wireless Propag. Lett.*, vol. 18, no. 6, pp. 1154-1158, Jun. 2019.

[15] A. H. Abdelrahman and D. S. Filipovic, "Antenna system for full-duplex operation of handheld radios," *IEEE Trans. Antennas Propag.*, vol. 67, no. 1, pp. 522-530, Jan. 2019.

[16] J. Zhou et al., "Integrated full duplex radios," *IEEE Commun. Mag.*, vol. 55, no. 4, pp. 142–151, Apr. 2017.

[17] M. Yilan, H. Ayar, H. Nawaz, O. Gurbuz, and I. Tekin, "Monostatic antenna in-band full duplex radio: performance limits and characterization," *IEEE Trans. Veh. Technol.*, vol. 68, no. 5, pp. 4786-4799, May. 2019.

[18] H. Nawaz and I. Tekin, "Dual-polarized, differential fed microstrip patch antennas with very high interport isolation for full-duplex communication," *IEEE Trans. Antennas Propag.*, vol. 65, no. 12, pp. 7355–7360, Dec. 2017.

[19] Y. Zhang and J. Li, "Differential-series-fed dual-polarized traveling-wave array for full-duplex applications," *IEEE Trans. Antennas Propag.*, vol. 68, no. 5, pp. 4097-4102, May. 2020.

[20] G. Srivastava and A. Mohan, "A differential dual-polarized SIW cavity-backed slot antenna," *IEEE Trans. Antennas Propag.*, vol. 67, no. 5, pp. 3450-3454, May. 2019.

[21] Z. Tang, J. Liu, R. Lian, Y. Li, and Y. Yin, "Wideband differentially fed dual-polarized planar antenna and its array with high common-mode suppression," *IEEE Trans. Antennas Propag.*, vol. 67, no. 1, pp. 131-139, Jan. 2019.

[22] B. Feng, X. He, J. Cheng, Q. Zeng, and C. Sim, "A low-profile differentially fed dual-polarized antenna with high gain and isolation for 5G microcell communications," *IEEE Trans. Antennas Propag.*, vol. 68, no. 1, pp. 90-99, Jan. 2020.

[23] Y. Zhang, S. Zhang, J. Li, and G. F. Pedersen, "A dual-polarized linear antenna array with improved isolation using a slotline-based 180° hybrid for full-duplex applications," *IEEE Antennas Wireless Propag. Lett.*, vol. 18, no. 2, pp. 348-352, Feb. 2019.

[24] W. Wang, J. Wang, A. Liu, and Y. Tian, "A novel broadband and high-isolation dual-polarized microstrip antenna array based on quasi-substrate integrated waveguide technology," *IEEE Trans. Antennas Propag.*, vol. 66, no. 2, pp. 951-956, Feb. 2018.

[25] Z. Chen, H. Liu, J. Yu, and X. Chen, "High gain, broadband and dual-polarized substrate integrated waveguide cavity-backed slot antenna array for 60 GHz band," *IEEE Access*, vol. 6, pp. 31012-31022, 2018.

[26] D. Kim, M. Zhang, J. Hirokawa, and M. Ando, "Design and fabrication of a dual-polarization waveguide slot array antenna with high isolation and high antenna efficiency for the 60 GHz band," *IEEE Trans. Antennas Propag.*, vol. 62, no. 6, pp. 3019-3027, Jun. 2014.

[27] S. J. Yang, Y. M. Pan, L. Shi, and X. Y. Zhang, "Millimeter-wave dual-polarized filtering antenna for 5G application," *IEEE Trans. Antennas Propag.*, vol. 68, no. 7, pp. 5114-5121, Jul. 2020.

[28] P. Li, S. Liao, Q. Xue, and S. Qu, "60 GHz dual-polarized high-gain planar aperture antenna array based on LTCC," *IEEE Trans. Antennas Propag.*, vol. 68, no. 4, pp. 2883-2894, Apr. 2020.

[29] Y. Li, C. Wang, and Y. X. Guo, "A Ka-band wideband dual-polarized magnetoelectric dipole antenna array on LTCC," *IEEE Trans. Antennas Propag.*, vol. 68, no. 6, pp. 4985-4990, Jun. 2020.

[30] N. Ashraf, A. R. Sebak, and A. A. Kishk, "Packaged microstrip line feed network on a single surface for dual-polarized 2N×2M ME-dipole antenna array," *IEEE Antennas Wireless Propag. Lett.*, vol. 19, no. 4, pp. 596-600, Apr. 2020.

[31] J. Liu, W. Zhou, and Y. Long, "A simple technique for open-stopband suppression in periodic leaky-wave antennas using two nonidentical elements per unit cell," *IEEE Trans. Antennas Propag.*, vol. 66, no. 6, pp. 2741-2751, Jun. 2018.

[32] A. Sarkar and S. Lim, "60 GHz compact larger beam scanning range PCB leaky-wave antenna using HMSIW for millimeter-wave applications," *IEEE Trans. Antennas Propag.*, vol. 68, no. 8, pp. 5816-5826, Aug. 2020.

[33] M. Al Sharkawy, A. Foroozesh, A. A. Kishk, and R. Paknys, "A robust horn ridge gap waveguide launcher for metal strip grating leaky wave antenna," *IEEE Trans. Antennas Propag.*, vol. 62, no. 12, pp. 6019-6026, Dec. 2014.

[34] N. Bayat-Makou, K. Wu, and A. A. Kishk, "Single-layer substrate-integrated broadside leaky long-slot array antennas with embedded reflectors for 5G systems," *IEEE Trans. Antennas Propag.*, vol. 67, no. 12, pp. 7331-7339, Dec. 2019.

[35] N. Bayat-Makou and A. A. Kishk, "Dual-layer substrate integrated broadside leaky-wave antenna," in *Proc. Global Symp. Millim. Waves (GSMM)*, Montreal, QC, Canada, May. 2015, pp. 1-3.

[36] N. Bayat-Makou, K. Wu, and A. A. Kishk, "Dual end-fed broadside leaky-wave antenna," U.S. Patent 20200203845, Jun. 25, 2020.

[37] P. Baccarelli, P. Burghignoli, D. Comite, W. Fuscaldo, and A. Galli, "Open-stopband suppression via double asymmetric discontinuities in 1-D periodic 2-D leaky-wave structures," *IEEE Antennas Wireless Propag. Lett.*, vol. 18, no. 10, pp. 2066-2070, Oct. 2019.

[38] D. M. Pozar, *Microwave Engineering*, 3rd ed. Hoboken, NJ, USA: Wiley, 2004.

[39] A. A. Oliner, and D. R. Jackson, "Leaky-Wave Antenna" in *Antenna Engineering Handbook*, 4th ed., J. Volakis, Ed. New York: McGraw-Hill, 2007.

[40] Y. Zhao and K. Luk, "Dual circular-polarized SIW-fed high-gain scalable antenna array for 60 GHz applications," *IEEE Trans. Antennas Propag.*, vol. 66, no. 3, pp. 1288-1298, Mar. 2018.

[41] Y. Li and K. Luk, "60-GHz dual-polarized two-dimensional switch-beam wideband antenna array of aperture-coupled magneto-electric dipoles," *IEEE Trans. Antennas Propag.*, vol. 64, no. 2, pp. 554-563, Feb. 2016.